ELSEVIER

Biophysical Chemistry 73 (1998) 249–263

Biophysical Chemistry

Deciphering the fluorescence signature of daunomycin and doxorubicin

Kerry K. Karukstis*, Elizabeth H.Z. Thompson, Jennifer A. Whiles, Robin J. Rosenfeld

Department of Chemistry, Harvey Mudd College, Claremont, CA 91711, USA

Received 9 February 1998; received in revised form 30 March 1998; accepted 30 March 1998

Abstract

The fluorescence characteristics of daunomycin (DNM), doxorubicin (DXR), and other anthracycline drugs are often used to monitor localization of the drug within lipid bilayers and liposomal delivery systems and to assess interaction of the drug with DNA and other macromolecules. However, the binding of DNM and DXR to proteins and membrane systems has been observed to exhibit variable effects on the anthracycline's fluorescence. We have delineated the spectroscopic response of DXR and DNM to their surroundings in several systems, including solvents of differing dielectric constant, aqueous solutions of varying pH or fluorophore concentration, and the reverse micellar system of AOT/heptane/water with a range of doxorubicin concentrations. We have observed that the ratio of fluorescence intensities at the two principal λ_{max} values shows a parabolic dependence on solvent dielectric constant, i.e. inverted solvatochromism. This behavior has been overlooked by previous investigators and, together with the appearance of a long-wavelength band near 630 nm in solvents of low dielectric strength (also previously not reported), is key to understanding the partitioning of anthracyclines in membrane systems as well as resolving the conflicting interpretation of data in the literature.

Keywords: Doxorubicin; Daunomycin; Solvatochromism; Fluorescence spectrum; Deconvolution; Reverse micelles

1. Introduction

The anthracycline anti-tumor drugs daunomycin (DNM) and doxorubicin (DXR) are potent anti-cancer drugs employed in chemotherapy. These amphiphilic molecules possess a fluorescent hydroxy-substituted anthraquinone chromophore and a hydrophilic aminoglycosidic side chain (see Fig. 1). The fluorescence characteristics of daunomycin and doxorubicin are often used to monitor their localization within lipid bilayers and liposomal delivery systems and their interaction

* Corresponding author. Tel.: +1 909 6073225; fax: +1 909 6077577; e-mail: Kerry_Karukstis@hmc.edu

0301-4622/98/$19.00
PII S0301-4622(98)00150-1

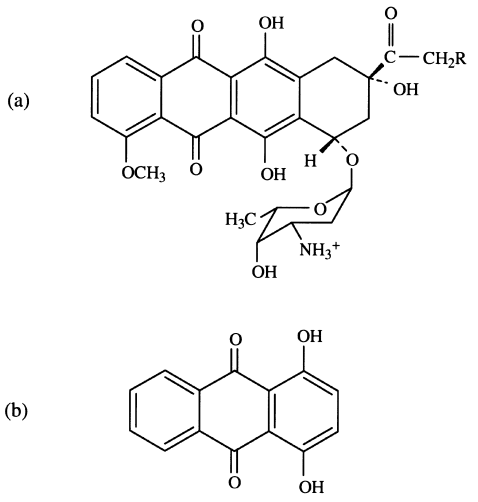

Fig. 1. Chemical structure of (a) daunomycin (R = H) and doxorubicin (R = OH), and (b) 1,4-dihydroxyanthraquinone.

with DNA and other macromolecules. Most often, the fluorescence intensity at the emission λ_{max} [1–5] and/or the ratio of fluorescence intensities at two characteristic wavelengths [5,6] are the parameters used to study and quantify these associations. However, the binding of daunomycin and doxorubicin to proteins and membrane systems has been observed to exhibit variable effects on DNM and DXR fluorescence. In some investigations fluorescence intensity increases upon binding [5,7,8], in other instances a quenching of fluorescence levels is observed [1–3,9–11]. Indeed, interaction of daunomycin with lipid systems can both diminish as well as enhance DNM fluorescence intensity depending on the drug/lipid ratio [12]. Incorporation of doxorubicin into the lipid matrix of model membranes has been observed to lead to both an increase and a decrease in the ratio of fluorescence intensities at the characteristic λ_{max} [5].

Despite the lack of regularity in response of DNM and DXR fluorescence, these fluorescence variations have each been attributed to an association of the drug with a less polar environment. In addition to the inconsistency in fluorescence intensity and ratio effects upon membrane partitioning, no uniformity exists in terms of the emission wavelength used to assess these interactions: emission has been monitored over the spectral range between 500 and 650–750 nm [4–6], only in the 558–570 nm region [1,9,10], only at 590 or 595 nm [2,3], or simply above 530–550 nm using longwavepass or cutoff filters [7,8,13]. Such assessments ignore the extreme wavelength dependence of the spectral signature of daunomycin and doxorubicin. Assessment of the site of drug localization with membranes and bilayers is often made assuming that the ratio of fluorescence intensities in the 560- and 590-nm regions is linearly dependent on the solvent dielectric constant ϵ, but this linearity has been tested only over a limited range of ϵ values [4–6]. As an additional consideration, investigators have made the incorrect assumption that the fluorescence spectrum of daunomycin is not affected by pH [1].

We have used various solvents, aqueous solutions of differing pH or drug concentration, and the reverse micellar system of surfactant Aerosol OT (AOT)/heptane/water to delineate the spectroscopic response of daunomycin and doxorubicin to their surroundings. For comparison, we examined the spectral response of the parent fluorophore 1,4-dihydroxyanthraquinone (1,4-diOH-AQ) to a range of solvents (see Fig. 1). Our spectroscopic investigations suggest that the distinctive fluorescence behavior of anthracyclines is a complex interplay of several factors. As a consequence, the intricate fluorescence signatures of these drugs are extremely sensitive and effective probes of their environment and their interaction with surfactants, lipids, and membranes.

In particular, we establish the importance of monitoring the overall fluorescence spectrum as well as the ratio of intensities at two λ_{max} values, near 560 nm and 590 nm, in order to assess daunomycin and doxorubicin microenvironment. Specifically, we demonstrate that the ratio of fluorescence intensities at the two λ_{max} values shows a parabolic dependence on solvent dielectric constant. We further note the appearance of a shoulder in the fluorescence spectrum of daunomycin and doxorubicin near 630 nm with decreasing solvent dielectric constant. These behaviors have been overlooked by previous investi-

gators and are key to understanding the partitioning of anthracyclines in reverse micelles as well as resolving the conflicting data in the literature.

2. Materials and methods

2.1. Materials

Daunomycin (DNM) and doxorubicin (DXR) were obtained as the hydrochlorides (Sigma) and were used without further purification. Solvents of the highest available purity were obtained commercially from Aldrich and J.T. Baker and were used without further purification. Aqueous stock solutions of DNM and DXR were prepared using 18.2 MΩ ultrapure water obtained from a Milli-Q Plus Millipore water filtration system. For reverse micelles, spectrophotometric grade *n*-heptane (Aldrich) and sodium bis(2-ethylhexyl) sulfosuccinate (AOT) (Sigma, > 99% purity) were used without further purification. Selected comparison studies were conducted with 1,4-dihydroxyanthraquinone (quinizarin, Aldrich, 96%) that was recrystallized twice from ethanol.

2.2. AOT reverse micelle preparation

We have previously characterized the reverse micellar aggregates formed by the double-chain surfactant Aerosol OT (sodium bis(2-ethylhexyl) sulfosuccinate, AOT) in the non-polar solvent heptane [14]. For the ternary system AOT/heptane/water, four distinct micellar regions are possible: the AOT interface, the surrounding hydrocarbon solvent phase, a 3–5 Å-thick 'bound water' layer immobilized via the hydration of the AOT headgroups and sodium counterions, and a 'free' water pool at the micellar core. We chose a surfactant concentration of [AOT] = 0.25 M and a molar ratio R of water to AOT (i.e. R = [water]/[AOT]) of 20 and 30 to insure the presence of all four micellar domains [14]. Samples were prepared by dissolving appropriate amounts of AOT in heptane and adding specific volumes of Millipore-filtered water to achieve the desired R value. Volume additivity was assumed in calculating AOT concentration and water/AOT molar ratios. Reverse micelle samples were allowed to stand overnight to establish phase equilibrium.

2.3. Fluorescence measurements

Fluorescence emission spectra were obtained using a Perkin-Elmer LS-50B fluorescence spectrophotometer. For solvents studies, fluorescence was induced by varying the excitation wavelength in 10-nm increments between 400 and 490 nm, and emission was monitored from 500 to 750 nm. For investigations involving reverse micelles, fluorescence was induced by excitation at 479 nm for DNM and DXR and at 474 nm for 1,4-diOH-AQ, and emission was monitored from 500 to 750 nm. Excitation and emission slit widths were set at 3 nm. Fluorescence measurements were made at 25 ± 2°C.

2.4. Fluorescence spectral analyses

A non-linear least-squares fitting routine (PeakFit, Jandel Scientific) was used to deconvolute individual emission spectra into a sum of overlapping Gaussian functions with frequency as the independent variable [15,16]. All spectra were fit using an iterative Marquardt-Levenberg fitting algorithm to obtain the minimum number of fluorescing components that yield an r^2 coefficient of at least 0.999 with a random scattering of residuals. The center, amplitude, width, and area of each Gaussian function were characterized.

3. Results

3.1. Resolution of DNM, DXR, and 1,4-diOH-AQ fluorescence in several solvents

We examined the emission of DNM and DXR in several solvents of varying polarity: water, deuterium oxide, ethylene glycol, methanol, ethanol, 1-propanol, isopentanol, 1-pentanol, 1-hexanol, 1-heptanol, 1-octanol, 1-decanol, ethyl acetate, *p*-dioxane, and heptane. As representative examples, Figs. 2 and 3 illustrate the dependence of the overall fluorescence emission spectrum of daunomycin on excitation wavelength in the sol-

vents water and 1-propanol at fixed [DNM]. For DNM and DXR in all solvents, two major emission maxima (denoted λ_1 and λ_2 with intensities I_1 and I_2) are observed at $\sim$555–560 nm and 590 nm with a third emission maximum (λ_3 with intensity I_3) resolved near 630 nm in solvents of lower dielectric constant. While overall fluorescence intensity varies with excitation wavelength, we observe little variation in spectral shape (i.e. constant values of λ_1, λ_2, λ_3, I_1/I_2, and I_3/I_2) for all solvents examined. Tables 1 and 2 summarize the characteristics of the major emission bands observed in all solvents with an excitation $\lambda = 479$ nm (selected for inducing maximal fluorescence intensities). As solubility of DNM and DXR varied with the particular solvent used, only the ratios of fluorescence intensities are reported. In general, the emission maxima at λ_1 and λ_2 exhibit a blue shift as solvent dielectric constant decreases. The data reveal a parabolic dependence of the ratio of intensities at 560 nm to 590 nm, decreasing from near 0.80 for water to 0.475 (DNM) at $\epsilon = 6$ and to 0.51 (DXR) at $\epsilon = 12$. Representative doxorubicin emission spectra (notably DXR in water, methanol, 1-pentanol, and heptane) are presented in Fig. 4 to illustrate further the spectral dependence on solvent.

Table 3 summarizes the characteristics of the parent fluorophore 1,4-dihydroxyanthraquinone (1,4-diOH-AQ) in several solvents. Two distinct emission λ_{max} values are observed: λ_1 exhibits a blue shift from 542 nm to 533 nm with decreasing dielectric constant (exception: *p*-dioxane), while λ_2 varies slightly but averages 566 ± 2 nm. The ratio of the fluorescence intensities at the λ_{max} near 540 nm and 565 nm is constant (average $\pm$ average deviation of 0.98 ± 0.01) over the range of solvents investigated except for heptane (ratio $= 1.05 \pm 0.02$). A shoulder near 610 nm is present for all solvents. Normalized emission spectra in representative solvents, namely, water, methanol, 1-pentanol, and heptane, appear in Fig. 5. Fig. 6 illustrates the dependence of I_1/I_2 on solvent dielectric constant for doxorubicin, daunomycin, and 1,4-dihydroxyanthraquinone.

The individual emission spectra of DXR in

Table 1
Emission characteristics of doxorubicin fluorescence in solvents of varying dielectric constant

Solvent	ϵ[a]	λ_1/nm[b]	λ_2/nm[b]	λ_3/nm[c]	I_1/I_2[e]	I_3/I_2[f]
Water	78.38	559	593	[d]	0.799	—
Deuterium oxide	78.25	563	595	[d]	0.734	—
Ethylene glycol	37.7	558	593	[d]	0.647	—
Methanol	32.66	554	588	[d]	0.624	—
Ethanol	24.3	555	588	[d]	0.575	—
1-Propanol	20.1	554	588	628	0.557	0.461
Isopentanol	14.7	556	590	631	0.530	0.456
1-Pentanol	13.9	554	590	629	0.533	0.452
1-Hexanol	13.3	554	590	631	0.541	0.446
1-Heptanol	12.1	554	590	633	0.514	0.450
1-Octanol	10.34	553	589	632	0.558	0.449
1-Decanol	8.1	553	589	633	0.562	0.455
Ethyl acetate	6.02	553	588	630	0.603	0.460
p-Dioxane	2.209	562	592	[d]	0.600	—
Heptane	1.924	551	589	628	1.08	0.506

Emission λ_{max} are reported for spectra obtained using an excitation wavelength of 479 nm. The ratios of the fluorescence intensities at the observed λ_{max} are also reported.
[a] Dielectric constants taken from [35].
[b] Uncertainty in emission wavelength maximum $\pm$ 1 nm.
[c] Uncertainty in emission wavelength maximum $\pm$ 2 nm.
[d] No additional distinct emission maxima observed.
[e] Maximum uncertainty in ratio of fluorescence intensities at λ_1 and $\lambda_2 \pm 0.007$.
[f] Maximum uncertainty in ratio of fluorescence intensities at λ_3 and $\lambda_2 \pm 0.007$.

Table 2
Emission characteristics of daunomycin fluorescence in solvents of varying dielectric constant

Solvent	ϵ[a]	λ_1/nm[b]	λ_2/nm[b]	λ_3/nm[c]	I_1/I_2[e]	I_3/I_2[f]
Water	78.54	560	592	[d]	0.800	—
Deuterium oxide	78.25	560	596	[d]	0.778	—
Ethylene glycol	38.66	561	592	[d]	0.641	—
Methanol	32.63	554	586	[d]	0.641	—
Ethanol	24.30	556	588	[d]	0.600	—
1-Propanol	20.1	552	588	631.5	0.569	0.45
Isopentanol	14.7	555	590	[d]	0.548	—
1-Pentanol	13.9	556	590	[d]	0.551	—
1-Hexanol	13.3	555	590	632	0.512	0.45
1-Heptanol	12.1	554	590	633	0.499	0.46
1-Octanol	10.3	554	589	634	0.514	0.43
1-Decanol	8.1	554	588	634	0.502	0.44
Ethyl acetate	6.02	555	588	628	0.475	0.52
p-Dioxane	2.209	562	592	[d]	0.620	—
Heptane	1.924	558	588	[d]	1.265	—

Emission λ_{max} are reported for spectra obtained using an excitation wavelength of 479 nm. The ratios of the fluorescence intensities at the observed λ_{max} are also reported.
[a] Dielectric constants taken from [35].
[b] Uncertainty in emission wavelength maximum $\pm$ 1 nm.
[c] Uncertainty in emission wavelength maximum $\pm$ 2 nm.
[d] No additional distinct emission maxima observed.
[e] Maximum uncertainty in ratio of fluorescence intensities at λ_1 and $\lambda_2 \pm 0.007$.
[f] Maximum uncertainty in ratio of fluorescence intensities at λ_3 and $\lambda_2 \pm 0.01$.

nine selected solvents were analyzed using the non-linear least-squares fitting routine in PeakFit, and Table 4 summarizes the characteristics (λ_{max} and % area of overall spectrum contributed by individual Gaussian curve) of the overlapping Gaussian functions resolved. Three principal

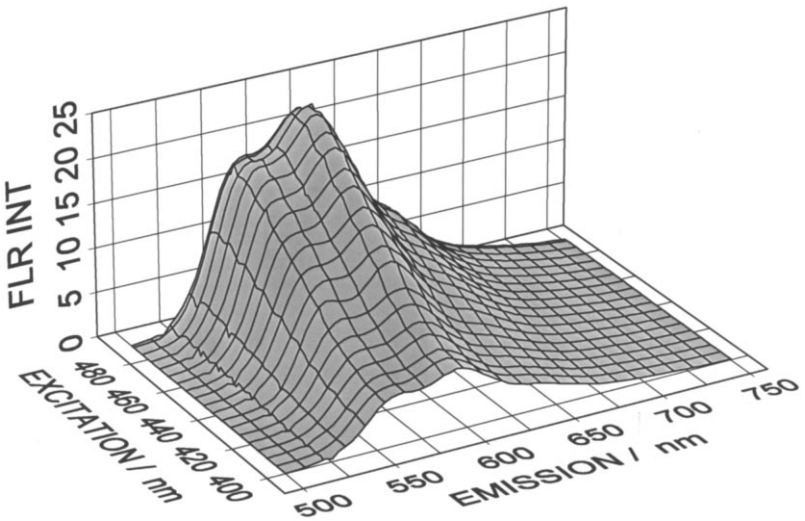

Fig. 2. The dependence of the fluorescence intensity of 10.0 μM daunomycin in water as a function of excitation and emission wavelengths.

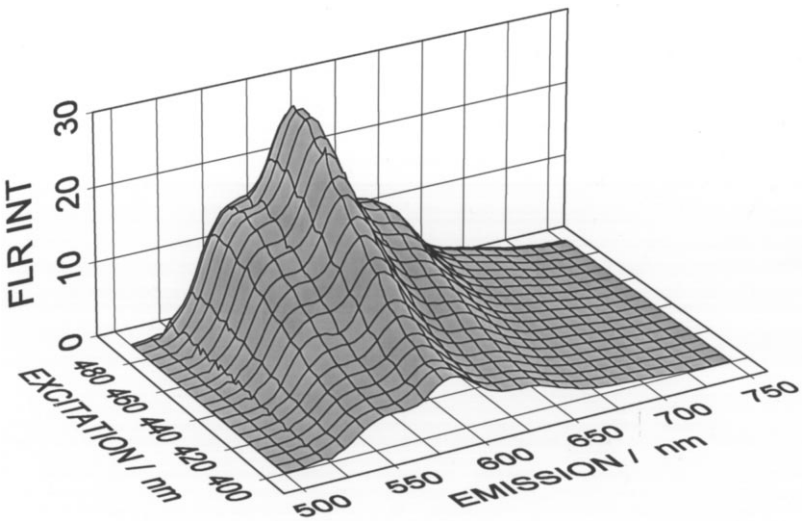

Fig. 3. The dependence of the fluorescence intensity of 5.0 μM daunomycin in 1-propanol as a function of excitation and emission wavelengths.

Gaussian curves are resolved, centered near 555 nm, 590 nm, and 635 nm, with a minor broad Gaussian peak at $\sim$670 nm. Fig. 7 illustrates the resolution of the doxorubicin fluorescence spectrum in isopentanol. As the dielectric constant of the solvent decreases, the most notable trends are: (1) general shifts in λ_{max} values to shorter wavelengths; (2) a steady increase in the percentage area of peak 3 at 630–635 nm from 14% to 21%; (3) a general decline in the percentage area of peak 1 at 550–555 nm as ϵ decreases to 14.7 (isopentanol), followed by an increase for solvents

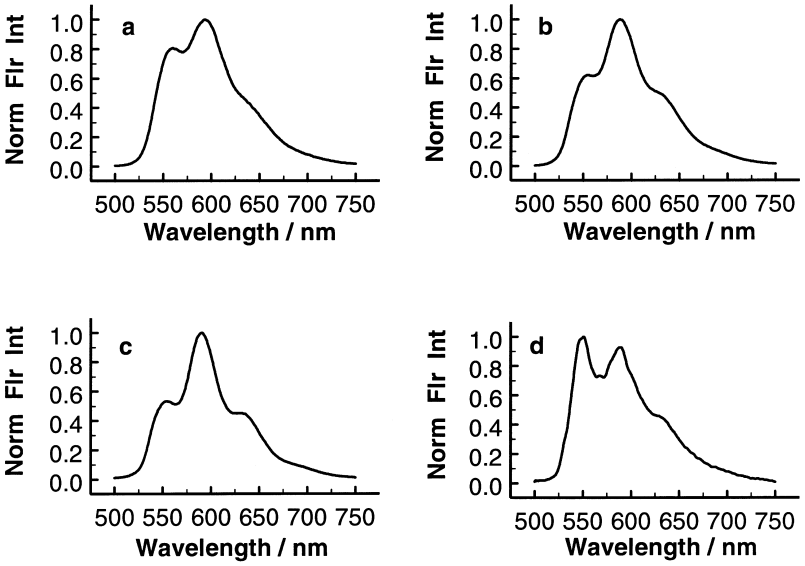

Fig. 4. Representative normalized emission spectra of doxorubicin in (a) water, (b) methanol, (c) 1-pentanol, and (d) heptane with excitation $\lambda = 479$ nm.

Table 3
Emission characteristics of 1,4-dihydroxyanthraquinone fluorescence in solvents of varying dielectric constant

Solvent	ϵ[b]	λ_1/nm[c]	λ_2/nm[c]	I_1/I_2[d]
Water	78.54	542	568	0.96
Deuterium oxide	78.25	544	567	0.98
Ethylene glycol	38.66	542	569	0.97
Methanol	32.63	535	563	0.97
Ethanol	24.30	534	565	0.98
Isopentanol	14.7	533	566	0.98
1-Pentanol	13.9	533	564	0.99
Ethyl acetate	6.02	534	568	0.97
p-Dioxane	2.209	542	567	0.99
Heptane[a]	1.924	532	562	1.05

Emission λ_{max} are reported for spectra obtained using an excitation wavelength of 474 nm. The ratios of the fluorescence intensities at the observed λ_{max} are also reported.
[a] Two additional peaks resolved at $\lambda_3 = 522$ nm ($I_3/I_2 = 0.89$) and $\lambda_4 = 544$ nm ($I_4/I_2 = 0.83$).
[b] Dielectric constants taken from [35].
[c] Uncertainty in emission wavelength maximum $\pm$ 1 nm.
[d] Maximum uncertainty in ratio of fluorescence intensities at λ_1 and λ_2 is $\pm$ 0.02.

of lower dielectric strength; and (4) the opposite trend for the % area of peak 2 at $\approx$ 590 nm with a general increase as ϵ decreases to 20–24 (ethanol and isopentanol), followed by a steady decrease for solvents of lower dielectric constant. The observed trend in the ratios of fluorescence intensities at 555 nm and 590 nm arises principally from the opposite variations in the contributions of peaks 1 and 2. Similar PeakFit analyses are obtained for daunomycin fluorescence as a function of solvent dielectric constant (results not shown).

PeakFit analyses of the fluorescence spectra of 1,4-dihydroxyanthraquinone also yield three principal Gaussian curves and a minor broad Gaussian peak at 658 ± 3 nm. Peak 1 shows a slight shift in λ_{max} from 535 ± 1 nm to 531 ± 2 nm as solvent ϵ decreases. Peaks 2 and 3 exhibit constant λ_{max} values of 566 ± 2 nm and 607 ± 2 nm. Area contributions of the four Gaussians remain constant as dielectric constant varies, at 32%, 44%, 20%, and 4% (all $\pm$ 1%) for peaks 1–4, respectively. The only exception is observed for heptane, where an additional Gaussian is resolved at 520 nm with 13% of the overall area, changing the contributions of peaks 1–4 to 18%, 47%, 17%, and 5%, respectively.

3.2. Dependence of DNM and DXR fluorescence on concentration

We examined the spectral dependence of DNM

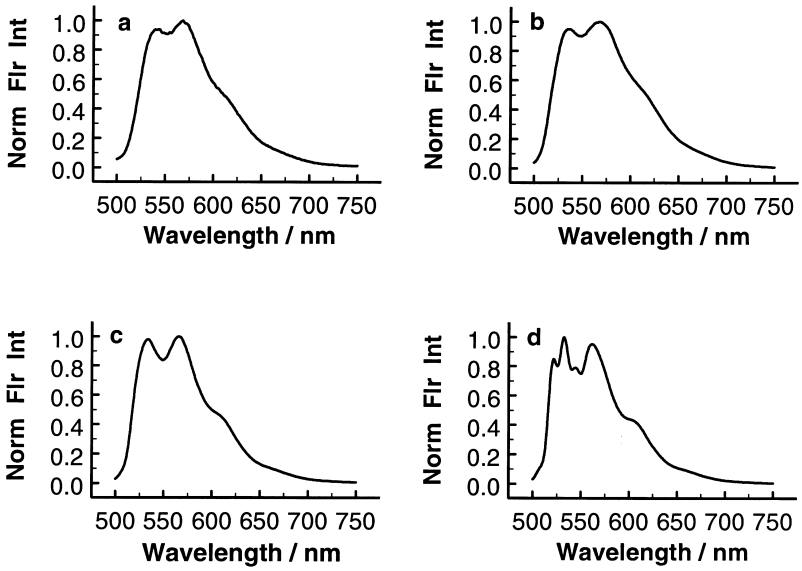

Fig. 5. Representative normalized emission spectra of 1,4-dihydroxyanthraquinone in (a) water, (b) methanol, (c) 1-pentanol, and (d) heptane with excitation $\lambda = 474$ nm.

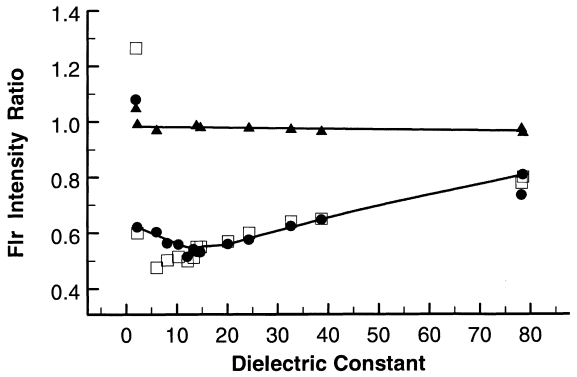

Fig. 6. The dependence on solvent dielectric constant of the ratio of the fluorescence intensities at the two principal emission λ_{max} values for doxorubicin (●), daunomycin (□), and 1,4-dihydroxyanthraquinone (▲). Corresponding data are tabulated in Tables 1, 2 and 3, respectively. The curve through the doxorubicin data is drawn to emphasize the occurrence of a minimum value for I_1/I_2. The line drawn through the 1,4-dihydroxyanthraquinone data is the average I_1/I_2 value (0.98) for all solvents except heptane.

fluorescence on [DNM] in water and in 1-propanol. The latter solvent was selected as an example of a non-polar solvent in which a third emission band (λ_3) is detected and in which DNM is soluble over a range of concentrations. In both solvent studies we also varied excitation wavelength over the range of 400–490 nm. Figs. 8 and 9 present the effect of [DNM] on (a) DNM absorbance, (b) the DNM fluorescence emission spectrum at an excitation λ of 480 nm, and (c) the maximal DNM fluorescence intensity at $\lambda_{excitation} = 480$ nm. In water, we observe the previously reported self-quenching of DNM fluorescence as a consequence of DNM self-association at concentrations greater than 10 μM [17]. In water over the [DNM] range of 3.35 to 16.75 μM, values of λ_1, λ_2, and I_1/I_2 are independent of excitation wavelength. The emission maxima at $\lambda_1 = 559 \pm 1$ nm and $\lambda_2 = 593 \pm 1$ nm are also independent of [DNM]. The ratio of the emission intensities at λ_1 and λ_2, I_1/I_2, decreases with increasing [DNM], from a value of 0.799 ± 0.006 at [DNM] = 3.35 μM to 0.775 ± 0.002 at [DNM] = 16.75 μM (averaged over all excitation wavelengths).

The concentration studies in 1-propanol also reveal a self-quenching of DNM fluorescence at higher [DNM], although the effect over the concentration range examined is not as pronounced as in water. In 1-propanol over the [DNM] range of 2.50 μM to 15.00 μM, values of λ_1, λ_2, λ_3, I_1/I_2, and I_3/I_2 are independent of excitation wavelength. The emission maxima at $\lambda_1 = 554 \pm 1$ nm, $\lambda_2 = 588 \pm 1$ nm, and $\lambda_3 = 628 \pm 1$ nm and the ratio of the emission intensities at λ_1 and λ_2, $I_1/I_2 = 0.557 \pm 0.002$, are also independent of

Table 4
PeakFit analysis of doxorubicin fluorescence emission spectra obtained in selected solvents

Solvent	Peak 1		Peak 2		Peak 3		Peak 4	
	λ/nm[a]	% Area[b]	λ/nm	% Area	λ/nm	% Area	λ/nm	% Area
Water	555	32.0	594	44.8	636	13.7	664	9.4
Deuterium oxide	555	32.1	596	44.5	640	14.6	671	8.8
Ethylene glycol	555	28.3	594	46.9	636	15.1	666	9.7
Methanol	550	26.1	588	45.8	630	13.7	652	14.5
Ethanol	550	26.0	589	47.4	631	17.6	668	9.0
Isopentanol	551	25.9	591	47.2	633	19.4	676	7.6
1-Pentanol	552	27.0	591	45.8	633	20.4	678	6.9
p-Dioxane	555	27.1	592	43.8	632	19.8	670	9.3
Heptane	549	34.6	586	39.2	629	21.0	674	5.2

Tabulated for each Gaussian curve resolved are (1) the center of the Gaussian peak and (2) the percentage area of the overall fluorescence spectrum that the peak contributes.
[a]λ_{max} values of resolved Gaussian curves reported to nearest nm.
[b]Area of each Gaussian curve reported as a percentage of the total emission spectrum. The sum of the % areas of the four Gaussian curves resolved may not add to 100% due to rounding.

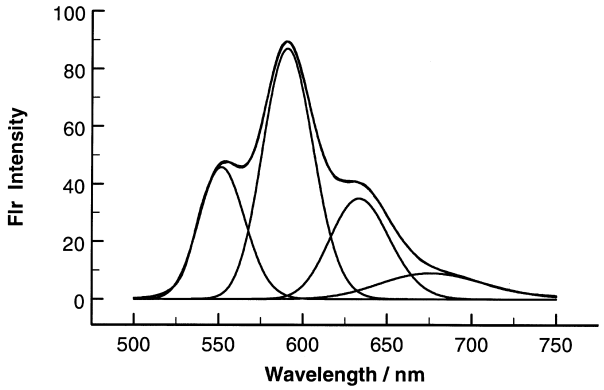

Fig. 7. Resolution of the doxorubicin fluorescence emission spectrum in isopentanol with excitation $\lambda = 479$ nm. Four overlapping Gaussian curves with centers at 551.5, 590.6, 633.3, and 675.7 nm and amplitudes of 45.78, 87.07, 34.93, and 8.97, respectively, contribute to the overall spectrum. The experimental emission spectrum and the theoretical fit to the experimental curve from the sum of the contributing Gaussian components are superimposed.

[DNM]. The ratio of the emission intensities at λ_3 and λ_2, I_3/I_2, decreases slightly with increasing [DNM], from a value of 0.469 ± 0.004 at [DNM] $= 2.50$ μM to 0.460 ± 0.001 at [DNM] $= 15.00$ μM (averaged over all excitation wavelengths).

The dependence of the DXR fluorescence emission spectrum on DXR concentration at a representative excitation wavelength of 479 nm is illustrated in Fig. 10. The emission λ_{max} values remain constant, with averages of 561 ± 1 nm and 593 ± 1 nm. The quenching of DXR fluorescence anticipated from the previously reported self-association of DNM at concentrations greater than 10 μM [17] is observed, giving rise to a small decline in the ratio of the peak intensities at 560 and 590 nm. (I_1/I_2 equals 0.804, 0.802, 0.787, and 0.775 ± 0.005 at [DXR] = 1.0, 5.0, 10.0, and 20.0 μM.) PeakFit analysis of the emission spectra reveal constant λ_{max} values averaging at $\lambda_1 = 555.2 \pm 0.3$ nm, $\lambda_2 = 593.8 \pm 0.2$ nm, $\lambda_3 = 637.3 \pm 0.6$ nm, and $\lambda_4 = 669 \pm 2$ nm. The % areas of both peaks 1 and 2 decrease slightly as [DXR] increases (from 31.1% to 29.8% for peak 1 and from 48.9% to 47.7% for peak 2, with uncertainties of $\pm 0.4\%$), while the % area of peak 3 remains essentially constant at $13.8 \pm 0.8\%$. Peak 4 is a minor component of constant contribution (% area $= 7.4 \pm 0.4\%$).

3.3. Dependence of DXR fluorescence on pH

Fig. 11 portrays the emission characteristics of 5 μM doxorubicin in aqueous samples of varying

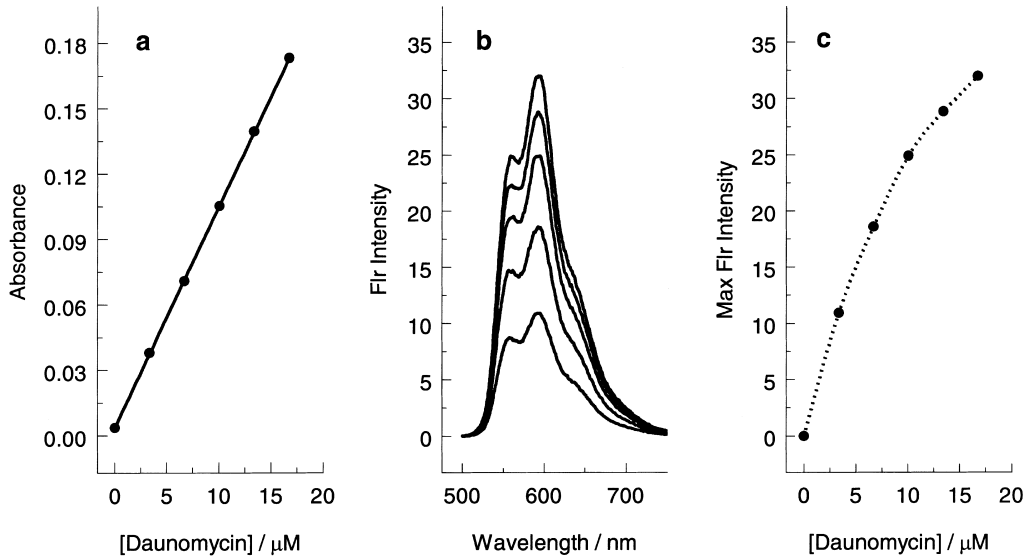

Fig. 8. The effect of [DNM] in water on (a) DNM absorbance, (b) the DNM fluorescence emission spectrum at an excitation λ of 480 nm, and (c) the maximal DNM fluorescence intensity at $\lambda_{excitation} = 480$ nm.

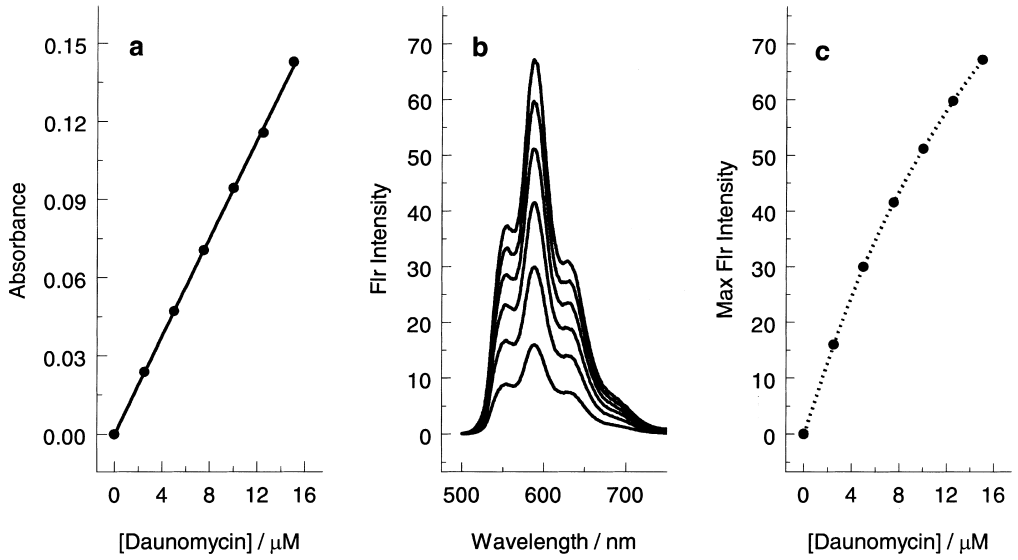

Fig. 9. The effect of [DNM] in 1-propanol on (a) DNM absorbance, (b) the DNM fluorescence emission spectrum at an excitation λ of 480 nm, and (c) the maximal DNM fluorescence intensity at $\lambda_{excitation} = 480$ nm.

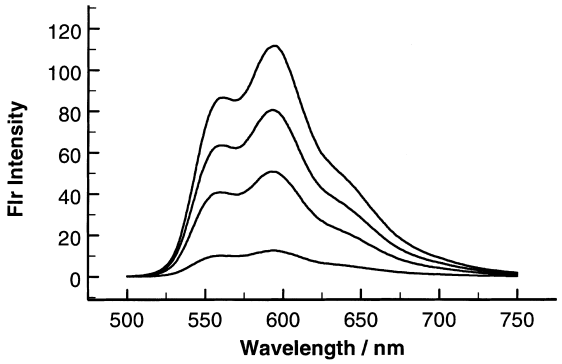

Fig. 10. The dependence of the doxorubicin fluorescence emission spectrum on the concentration of DXR in aqueous solution. As spectra increase in intensity, the doxorubicin concentration corresponds to 1.0, 5.0, 10.0, and 20.0 μM.

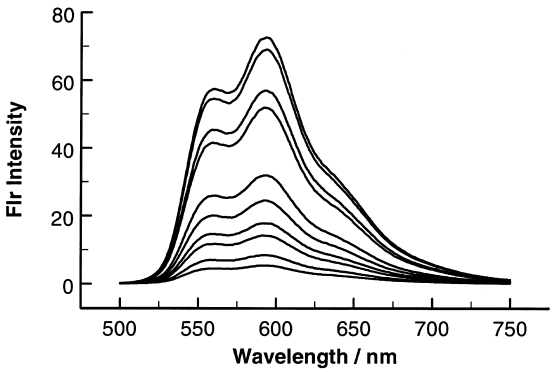

Fig. 11. Fluorescence of 10 μM doxorubicin as a function of pH with excitation $\lambda = 479$ nm. The peak emission intensities occur at $\lambda_1 = 560 \pm 1$ nm and $\lambda_2 = 593 \pm 1$ nm. The ratio of fluorescence intensities at λ_1 and λ_2 (I_1/I_2) increases with increasing pH: $I_1/I_2 = 0.790$ at pH 5.52; 0.790, pH 6.37; 0.796, pH 6.55; 0.799, pH 6.92; 0.812, pH 8.51; 0.818, pH 9.01; 0.823, pH 9.33; 0.821, pH 9.61; 0.827, pH 10.10; 0.840, pH 10.40. Maximum uncertainty in I_1/I_2 is ± 0.005, except for pH values > 10, ± 0.010.

pH. The range of pH values investigated was selected to span the pK_a of the glycosidic amine, with reported values varying from 7.4 to 8.2 [18–21]. However, a simultaneous dissociation of a phenolic group on the anthraquinone ring is possible, as the phenolic group is known to ionize over the pH range 8 to 13 [18]. A marked decrease in fluorescence intensity at both emission λ_{max} values is observed, with no shift in the location of λ_{max} at 560 ± 1 nm and 593 ± 1 nm. The ratio of intensities (I_1/I_2) shows a slight increase with more basic solution, from $I_1/I_2 = 0.790$ at pH 5.52 to $I_1/I_2 = 0.840$ at pH 10.40. Daunomycin fluorescence exhibits a similar dependence on pH, with decreasing intensity as pH rises, constant emission λ_{max} values at $\lambda_1 = 564 \pm 2$ nm

and $\lambda_2 = 594 \pm 1$ nm, and a small increase in I_1/I_2 from 0.80 at pH 5.0 to 0.83 at pH 9.0.

PeakFit analysis of the DXR pH data reveals four Gaussian curves that decrease in amplitude with increasing pH while maintaining a constant percentage area and constant λ_{max} values. The average λ_{max} values (and average % areas) of the resolved Gaussians occur at $\lambda_1 = 554.8 \pm 0.3$ nm ($30.5 \pm 0.2\%$), $\lambda_2 = 593.5 \pm 0.1$ nm ($48.5 \pm 0.6\%$), $\lambda_3 = 637.3 \pm 0.5$ nm ($14.3 \pm 0.7\%$), and $\lambda_4 = 672 \pm 3$ nm ($6.7 \pm 0.6\%$). The two major Gaussian bands exhibit a constant ratio of peak amplitudes (amplitude$_1$:amplitude$_2 = 0.740 \pm 0.007$). The intensity of the peak at 593.5 nm exhibits a more sizable pH dependence (decreasing more significantly with increasing pH than the intensity of the 554.8-nm peak), giving rise to the observed increase in the ratio of fluorescence intensities at λ_1 and λ_2.

3.4. Resolution of DXR fluorescence in AOT/n-heptane/water reverse micelles as a function of DXR concentration

The experimentally-determined fluorescence parameters of DXR in AOT/heptane/water reverse micelles ($R = 20$ and 30) are presented in Table 5. Little variation is observed in the emission λ_{max} values, but a significant decrease in the magnitude of the ratio of the fluorescence intensities at 557 nm and 590 nm (I_1/I_2) is revealed. The value of I_1/I_2 is close to or above 1 at low concentrations of DXR, falling to near 0.74 at the highest DXR concentrations investigated. Normalized fluorescence emission spectra at 0.10 μM and 20.0 μM DXR ($R = 30$) are presented for comparison in Fig. 12.

PeakFit analysis of the fluorescence spectra at $R = 30$ are summarized in Table 6. As expected, three principal Gaussian curves are resolved with a minor long-wavelength component. The 555-nm and 590-nm components show little variation in emission wavelength, while the third Gaussian displays an increase in emission wavelength as [DXR] increases. The more dramatic variations with [DXR] are observed for the % areas of the Gaussian peaks, decreasing for the 555-nm and 630-nm peaks and increasing for the 590-nm Gaussian. The ratio of both amplitudes and % areas for the 555-nm and 590-nm peaks shows a gradual decrease with increasing [DXR].

Table 5
Emission characteristics of doxorubicin fluorescence in AOT/heptane/water reverse micelles as a function of DXR concentration

[DXR]/μM	λ_1/nm[a]	I_1	λ_2/nm[a]	I_2	I_1/I_2[b]
$R = 20$					
0.05	557	1.10	589	0.942	1.17
0.10	558	1.93	586	1.83	1.05
0.20	558	2.81	590	3.22	0.87
0.30	556	3.48	591	4.10	0.85
0.40	558	5.04	590	6.20	0.81
0.50	559	5.88	590	7.30	0.80
1.0	556	11.8	590	15.3	0.77
5.0	556	49.3	591	65.3	0.75
10.0	558	86.0	590	115.3	0.75
$R = 30$					
0.10	557	1.90	590	2.00	0.95
0.25	556	5.24	590	6.19	0.85
0.50	556	6.77	590	8.39	0.81
0.75	556	9.90	592	12.4	0.80
1.0	557	12.3	590	15.8	0.78
5.0	556	48.3	590	63.1	0.77
10.0	558	90.0	592	118.6	0.76
20.0	560	150.9	591	204.2	0.74

Emission λ_{max} are reported for spectra obtained using an excitation wavelength of 479 nm. Doxorubicin concentration is varied in reverse micelles with fixed [AOT] = 0.25 M and molar ratios of water to surfactant of 20 and 30. The ratios of the fluorescence intensities at the observed λ_{max} are also reported.

[a] Uncertainty in emission wavelength maximum $\pm$ 1 nm.

[b] Maximum uncertainty in ratio of fluorescence intensities at λ_1 and $\lambda_2 \pm 0.01$.

The neutral, non-polar character of 1,4-diOH-AQ dictates a preferential partitioning of the fluorophore into only the heptane bulk solvent of the AOT/heptane/water reverse micellar system. A fluorescence spectrum that matched identically to that of 1,4-diOH-AQ in heptane solvent was observed for AOT reverse micelles with added 1,4-diOH-AQ despite variations in [AOT] over the range from 0.10 M to 0.25 M, changes in water content from $R = 20$ to 35, and [1,4-diOH-AQ] values ranging from 2 to 10 μM.

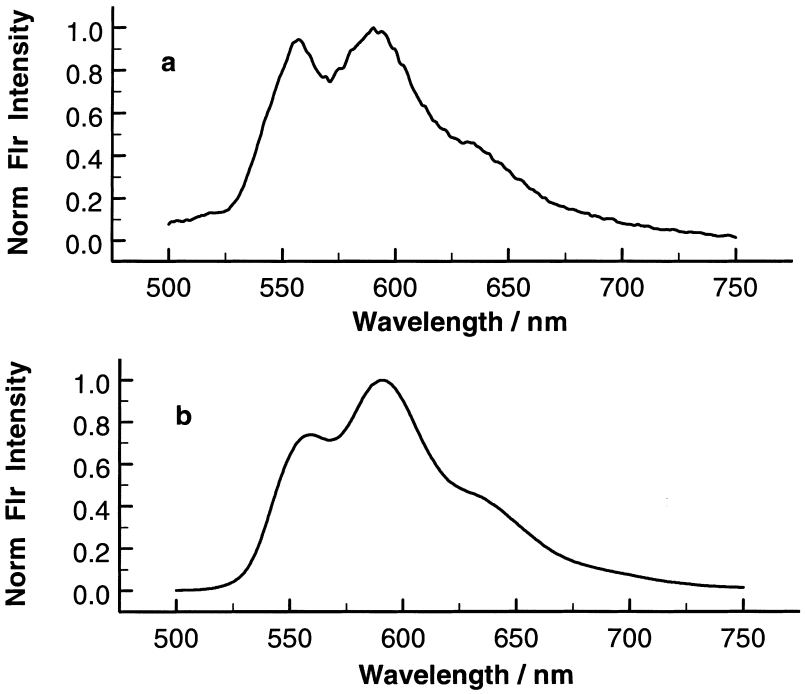

Fig. 12. Normalized fluorescence emission spectra at (a) 0.10 μM and (b) 20.0 μM DXR in the reverse micellar system AOT/heptane/water at [AOT] = 0.25 M, $R = 30$, and excitation $\lambda_{max} = 479$ nm.

4. Discussion

Several key fluorescence spectral characteristics of daunomycin and doxorubicin emerge from this study. (1) Two principal emission λ_{max} values are observed, occurring at $\sim \lambda_1 = 560$ nm and $\lambda_2 = 593$ nm in aqueous solution and exhibiting blue shifts of ~ 5 nm in solvents of low dielectric constant. (The parent fluorophore 1,4-dihydroxyanthraquinone also exhibits two emission λ_{max} values, with λ_1 exhibiting a similar blue shift of up to 10 nm with decreasing solvent dielectric constant.) In aqueous solution, no variations in DXR and DNM emission λ_{max} are observed for changes in pH or fluorophore concentration. (2) A long-wavelength shoulder near 630 nm is more pronounced in solvents of lower dielectric strength and shows no variation with solution pH or fluorophore concentration. (The parent fluorophore 1,4-diOH-AQ exhibits a long-wavelength shoulder in the emission spectrum in all solvents.) (3) The peak ratio of fluorescence intensity at short λ_{max} (560 nm) to long λ_{max} (593 nm) can be significantly varied by a change in the solvent dielectric constant and slightly altered by a change in the pH of the environment or in the local concentration of DXR or DNM.

In particular, the DXR and DXR fluorescence peak ratio is decreased by (a) increased effective DXR concentration and (b) decreased pH of the surroundings. In contrast, by an investigation of solvents with an extensive range of dielectric constants, we have demonstrated that the ratio of fluorescence intensities at the two λ_{max} values shows a parabolic dependence on solvent dielectric constant. As dielectric constant decreases from the value for water, the ratio of fluorescence intensity at 560 nm to that at 593 nm decreases to a minimum value at a dielectric constant in the vicinity of $\epsilon = 6$ (for the more hydrophobic DNM) and 12 (for DXR with an additional hydroxyl group) and then increases with continually decreasing dielectric constant to a ratio above the value observed for water. This unusual inverted

Table 6
PeakFit analysis of doxorubicin fluorescence spectra obtained for AOT/heptane/water reverse micelles at $R = 30$ with varying DXR concentration

[DXR]	Peak 1			Peak 2			$Ampl_1$:	Peak 3			Peak 4		
	λ/nm	Ampl	% Area	λ/nm	Ampl	% Area	$Ampl_2$	λ/nm	Ampl	% Area	λ/nm	Ampl	% Area
0.10	555	1.60	36.4	590	1.60	34.9	1.00	628	0.79	26.7	692	0.08	1.98
0.25	554	4.68	33.3	590	5.49	41.3	0.852	632	2.39	23.8	690	0.27	1.56
0.50	554	6.10	32.3	590	7.53	42.6	0.810	629	3.23	23.1	690	0.40	1.92
0.75	554	8.93	31.0	591	11.64	45.6	0.767	634	4.72	20.6	687	4.72	2.72
1.0	554	11.04	30.6	591	14.89	47.0	0.741	634	5.83	19.8	686	0.93	2.72
5.0	554	43.71	29.8	591	60.48	47.8	0.723	634	22.22	16.9	676	5.51	5.47
10.0	554	80.91	29.4	591	114.1	47.6	0.709	634	42.04	17.4	676	10.52	5.66
20.0	555	134.6	28.8	591	194.4	46.7	0.692	633	76.02	19.1	678	17.42	5.45

The center[a] and amplitude[b] of each Gaussian curve resolved are tabulated as well as the percentage area[c] of the overall fluorescence spectrum that the peak contributes. The ratio of the amplitudes of the Gaussians at λ_1 and λ_2 is also tabulated[d].
[a]λ_{max} values of resolved Gaussian curves reported to nearest 0.1 nm.
[b]Amplitudes of resolved Gaussian curves reported to nearest 0.01.
[c]Area of each Gaussian curve reported as a percentage of the total emission spectrum. The sum of the % areas of the four Gaussian curves resolved may not add to 100% due to rounding.
[d]Maximum uncertainty in ratio of amplitudes at λ_1 and $\lambda_2 \pm 0.004$.

solvatochromism — that is, a reversal of solvatochromic shifts in media of low polarity — has been previously observed for several merocyanine dyes [22–24] and a class of bischromophoric cyanine dyes [25]. Observing this behavior is key to understanding the partitioning of anthracyclines in reverse micelles as well as resolving the conflicting data in the literature.

Several stabilizing factors are likely to influence the localization of doxorubicin within the microregions of reverse micelles. In the partitioning process the fluorophore could attempt to enhance the solvation and hydrogen bonding of the hydrophilic aminoglycosidic side chain, optimize the electrostatic interactions of the protonated amine, and/or maximize the hydrophobic and cation-π interactions of the anthraquinone ring system with the surfactant interface. These driving forces can modulate both the orientation of the anthracycline drug with respect to the surfactant (parallel vs. tangential) and the depth of penetration of the aromatic moiety into the surfactant layer for parallel orientations.

Our reverse micelle investigations suggest that the partitioning of DXR in AOT reverse micelles of fixed composition is dependent on the concentration of doxorubicin. Two critical trends used to support this proposal are (1) the varying intensity ratio I_1/I_2 of the emission peaks at 555 and 590 nm as the concentration of DXR increases and (2) the shift in wavelength and the change in % area of peak 3 (near 630 nm) in the PeakFit analysis of the emission spectra as [DXR] increases. Using the data in Tables 1 and 4 to assist in interpretation, a possible partitioning scenario may be constructed.

At low drug concentrations, the chromophore of doxorubicin appears to reside in an hydrophobic environment (presumably the surfactant interface). The high I_1/I_2 ratio coupled with the relatively short emission wavelength of peak 3 and its large % contribution are consistent with a hydrophobic site for the chromophore. At higher concentrations, doxorubicin partitions into a more hydrophilic environment such as either the free water pool or the bound water layer. A decrease in the depth of partitioning into the surfactant layer would also be consistent with a more hydrophilic site. The lower I_1/I_2 value and the longer wavelength for peak 3 and its smaller area contribution to the overall spectrum suggest this more hydrophilic region. A similar concentration-dependent partitioning of doxorubicin into anionic unilamellar vesicles has been suggested

[26]. In this earlier study, the chromophore of DXR at low concentrations is proposed to intercalate between the lipid molecules, while at high concentrations drug–drug interactions cause the protrusion of additional DXR chromophores at least partly into the aqueous phase.

Our observation of the parabolic dependence of the daunomycin and doxorubicin 560-nm:593-nm fluorescence ratios may offer an explanation for the apparent paradoxical assignment of a more aqueous partitioning site in large unilamellar vesicles for the more hydrophobic idarubicin (and its derivatives 3′-hydroxyidarubicin and idarubicinol) than for daunomycin or doxorubicin [5]. This assignment (which the authors noted was not consistent with the hydrophobicity of idarubicin) was made on the basis of relative fluorescence intensity ratios (I_1/I_2) and the assumption that I_1/I_2 decreases with decreasing solvent dielectric constant. (The data presented [5] to support the latter point showed considerable deviation from a linear dependence.) In light of our findings, the observed [5] fluorescence ratios in the range of 0.91–1.02 should be ascribed to a more hydrophobic location for the chromophore of idarubicin and its derivatives, consistent with an embedding of the anthraquinone moiety within the surfactant region. This example emphasizes the necessity, as revealed by our investigations, of using both overall spectral shape (particularly the contribution of a Gaussian emission band centered near 630 nm) and the intensity ratios at the principal λ_{max} values (560 and 590 nm) to assess the location of DXR and DNM in lipid and surfactant systems.

A full characterization of the fluorescence signature of daunomycin and doxorubicin is critical for the assessment of anthracycline distribution in cell membranes. While interference of nucleic acid function is the classical model to explain the therapeutic activity of these anthracyclines [27,28], the interactions of the drugs with cell membranes are also critical to their overall function. Drug-membrane interactions govern cytotoxic selectivity between normal and tumor tissue, dictate cell access, and are implicated in the development of multiple drug resistance by tumor cells. Partitioning of the drugs between membrane and cystolic fractions of cells significantly favors the membrane, yet higher quantities of lipid-bound anthracyclines are observed in drug-sensitive cells than in resistant cells [29–32]. The detection of different distributions of these anthracyclines in membranes from drug-sensitive and drug-resistant cells suggest differential partitioning of the drug between ‘deep’ (membrane-incorporated) and ‘surface’ domains as a consequence of variations in the concentrations of certain lipids [33,34]. Clearly, a greater understanding of anthracycline–membrane interactions is fundamental to optimizing anthracycline activity. We are continuing to use fluorescence spectroscopy to investigate the partitioning of DNM and DXR in surfactant-based reverse micellar systems to provide further understanding of the binding heterogeneity of these anthracyclines in biological membranes and liposomal delivery systems.

Acknowledgements

The authors acknowledge the support of a National Institutes of Health Academic Research Enhancement Award (1 R15 GM/OD55911). This research was also supported in part by a grant from the National Science Foundation Research Experiences for Undergraduates Program (CHE-9322804). K.K.K. also acknowledges support from a Henry Dreyfus Teacher-Scholar Award.

References

[1] S. Simon, D. Roy, M. Schindler, Proc. Natl. Acad. Sci. USA 91 (1994) 1128.
[2] C.J. Roche, J.A. Thomson, D.M. Crothers, Biochemistry 33 (1994) 926.
[3] C.J. Roche, D. Berkowitz, G.A. Sulikowski, S.J. Danishefsky, D.M. Crothers, Biochemistry 33 (1994) 936.
[4] N. Husain, T.T. Ndou, A. Munoz de la Pena, I.M. Warner, Appl. Spect. 46 (1992) 652.
[5] L. Gallois, M. Fiallo, A. Laigle, W. Priebe, A. Garnier-Suillerot, Eur. J. Biochem. 241 (1996) 879.
[6] R. Goldman, T. Facchinetti, D. Bach, A. Raz, M. Shinitzky, Biochim. Biophys. Acta 512 (1978) 254.
[7] T.G. Burke, T.R. Tritton, Biochemistry 24 (1985) 1768.
[8] V. Rizzo, N. Sacchi, M. Menozzi, Biochemistry 28 (1989) 274.

[9] L.E. Xodo, G. Manzini, J. Ruggiero, Biopolymers 27 (1988) 1839.
[10] J. Lankelma, H.S. Mulder, F. van Mourik, H.W. Wong Fong Sang, R. Kraayenhof, R. van Grondelle, Biochim. Biophys. Acta 1093 (1991) 147.
[11] F. Barcelo, I. Barcelo, F. Gavilanes, J.A. Ferragut, S. Yanovich, J.M. Gonzalez-Ros, Biochim. Biophys. Acta 884 (1986) 172.
[12] F.G. Sanchez, C.C. Ruiz, J. Lumin. 55 (1993) 321.
[13] T.G. Burke, T.R. Tritton, Anal. Biochem. 143 (1984) 135.
[14] K.K. Karukstis, A.A. Frazier, D.S. Martula, J.A. Whiles, J. Phys. Chem. 100 (1996) 11133.
[15] P.A. Jansson (Ed.), Deconvolution with Applications in Spectroscopy, Academic Press, Orlando, FL, 1984, p. 35.
[16] G.W. Halsey, W.E. Blass, in: P.A. Jansson (Ed.), Deconvolution with Applications in Spectroscopy, Academic Press, Orlando, FL, 1984, p. 187.
[17] J.B. Chaires, N. Dattagupta, D.M. Crothers, Biochemistry 21 (1982) 3927.
[18] R.J. Sturgeon, S.G. Schulman, J. Pharm. Sci. 66 (1977) 958.
[19] S. Eksborg, J. Pharm. Sci. 67 (1978) 782.
[20] P.G. Righetti, M. Menozzi, E. Giannazza, L. Valentini, FEBS Lett. 101 (1979) 51.
[21] I.J. McLennan, R.E. Lenkinski, Y. Yanuka, Can. J. Chem. 63 (1985) 1233.
[22] P. Jacques, J. Phys. Chem. 90 (1986) 5535.
[23] M. Niedbalska, I. Gruda, Can. J. Chem. 68 (1990) 691.
[24] C. Aliaga, J.S. Galdames, M.C. Rezende, J. Chem. Soc. Perkin Trans. 2 (1997) 1055.
[25] B.K. Mishra, M. Kuanar, A. Mishra, G.B. Behera, Bull. Chem. Soc. Jpn. 69 (1996) 2581.
[26] F. de Wolf, M. Maliepaard, F. van Dorsten, I. Berghuis, K. Nicolay, B. de Kruijff, Biochim. Biophys. Acta 1096 (1991) 67.
[27] F. Arcamone, in: A.C. Sartorelli (Ed.), Doxorubicin: Anticancer Antibiotics, Academic Press, New York, 1981, p. 1.
[28] M.J. Waring, Annu. Rev. Biochem. 50 (1981) 159.
[29] C. Myers, K. Gowan, B. Sinha, B. Chabner, in: V.T. DeVita, S. Hellman, S.A. Rosenberg (Eds.), Important Advances in Oncology, J.B. Lippincott Co., Philadelphia, 1987, p. 27.
[30] G. Bradley, P.F. Juranka, V. Ling, Biochim. Biophys. Acta 948 (1988) 87.
[31] S. Awasthi, R. Sharma, Y.C. Awasthi, J.A. Belli, E.P. Frenkel, Cancer Lett. 63 (1992) 109.
[32] S. Drori, G.D. Eytan, Y.G. Assaraf, Eur. J. Biochem. 228 (1995) 1020.
[33] P. Escriba, A.V. Ferrer-Montiel, J.A. Ferragut, J.M. Gonzalez-Ros, Biochemistry 29 (1990) 7275.
[34] A.V. Ferrer-Montiel, J.M. Gonzalez-Ros, J.A. Ferragut, Biochim. Biophys. Acta 1104 (1992) 111.
[35] D.R. Lide (Ed.), Handbook of Chemistry and Physics, 74th edn., CRC Press, Boca Raton, FL, 1993.